COBEM 2021 26th International Congress of Mechanical Engineering
ABCM Associação Brasileira de Engenharia e Ciências Mecânicas
November 22-26, 2021, Virtual Congress, Brazil

FLUID-STRUCTURE INTERACTION FOR CANTILEVER PLATES IMMERSED IN AIR AND WATER USING SOLID ELEMENT IN STRUCTURE SUBSYSTEM ON MFSIM (IN-HOUSE SOFTWARE)

Freddy Alejandro Portillo Morales
alejandro@ufu.br

Aristeu da Silveira Neto
aristeus@ufu.br

Aldemir Aparecido Cavallini Jr.
Federal University of Uberlandia - Av. Joao Naves de Avila, 2121. Uberlandia, MG, Brasil
aacjunior@ufu.br

Abstract. *Numerical simulation has advanced rapidly over the past decade, and new mathematical and computational models have emerged in order to describe the physics of problems with greater fidelity. This work addresses a fluid-structure interaction problem in a partitioned way, solving the fluid subsystem and the structure subsystem separately. The first is solved using the Finite Volume Method (FVM) and the second with the Finite Element Method (FEM), using the immersed boundary method (IBM) to communicate these two subsystems. For the discretization of the structure subsystem, Hexa-8 with incompatible modes solid elements are used, this type of elements allows the modeling of complex geometries that could not be modeled with beam and plate elements. Virtual experiments were carried out and compared with the results obtained experimentally by Lindholm* et al. *(1965). The experiments consisted of applying an instantaneous force to the free end of the plate (pluck test) and measuring its displacements over time, these data are treated with the use of a Fast Fourier Transform (FFT) and thus obtained the natural frequencies of the structure taking into account the effects of the fluid in which it is immersed. The results obtained were satisfactory, the maximum errors obtained in relation to the material experiment were 4.74 % for plates in a vacuum, 8.85 % for plates submerged in air and 14.55 % for plates submerged in water. The validation of these preliminary results is part of the implementation of solid elements in the MFSim, in-house code, developed by the Fluid Mechanics Laboratory (MFLab) of the Federal University of Uberlandia (UFU) in partnership with Petrobras.*
Keywords: *Fluid-structure interaction, Vibration response, Incompatible modes.*

1. INTRODUCTION

The fluid-structure interaction (FSI) is characterized by the interaction of one or more solid bodies with an internal or external fluid flow. Several examples are found both in natural systems and in objects built by humans. The airflow through trees is an example of a natural system under fluid-structure interaction, on the other hand, in engineering it is possible to appreciate the fluid-structure interaction in the airflow around the wing of a moving plane, platforms (off-shore) in the middle of the ocean or wind turbines.

FSI problems are multidisciplinary, they mainly involve the fields of fluid dynamics and solid dynamics, and can be studied in a material or virtual experimental way. For any type of study, the physical modeling of the problem is necessary, which consists of a detailed evaluation of the case under study and the determination of the physical assumptions that allow for the simplification of the problem, enabling its analysis. The virtual experiment consists of the mathematical and computational modeling of the case, as well as the use of numerical methods to discretize the equations that model the physics of the problem. The use of computer simulation techniques to solve physical problems has grown together with the advancement of computational tools, the increase in data storage capacity and the speed of processing operations, thus allowing heavier and more robust cases to be analyzed. It is noteworthy that the computational method does not replace the material experiments, but they complement each other.

To be able to mathematically analyze FSI problems it is necessary to perform a coupling between the fluid system and the structural system. According to Sotiropoulos and Yang (2014) it is possible to carry out this coupling in two ways, monolithic coupling or partitioned coupling. In monolithic coupling the two subsystems are solved in a single linear system simultaneously. Partitioned coupling requires the resolution of each subsystem separately and coupled through their boundary conditions at each time step, and these can be divided into weak and strong couplings. This partitioned coupling approach is the methodology used for the present work, allowing to solve the fluid subsystem through the Finite Volume Method (FVM) and the structural subsystem through the Finite Element Method (FEM).

For the FEM it is proposed the implementation of computational algorithms for the use of solid type elements, more specifically hexahedral elements of 8 nodes with extra shape functions (Hexa-8 ESF) or also known as incompatible elements. This implementation will be performed in the in-house code, MFSim, from the Fluid Mechanics Laboratory (MFLab).

2. METHODOLOGY

In the present work computational simulations of plates submerged in water and air are performed. The numerical mathematical model used to evaluate the problem under study is presented below.

2.1 Vibrational response of cantilever plates submerged in water and air

This work aims to validate the implementations carried out in MFSim with the case of fluid-structure interaction for cantilever plates submerged in water and air. The results obtained are compared with the results of the material experiment carried out by Lindholm *et al.* (1965). Four plates were chosen for the evaluation of displacements at the free end after applying an instantaneous force (Pluck test). After applying instantaneous force, the plates vibrate freely for 5 physical seconds. The plates were discretized using the three-dimensional element Hexa-8 ESF. The dimensions of the plates tested are as follows in Tab. 1. The information on the meshes generated for both the fluid and the structural subsystems are displayed in Tab 2.

Table 1. Dimensions of the tested plates (Lindholm *et al.*, 1965)

Plate	Side a (mm)	Side b (mm)	h Thickness (mm)
Lind-5	203,2	203,2	4,83616
Lind-6	406,4	203,2	4,83616
Lind-7	609,6	203,2	4,83616
Lind-8	1016,0	203,2	4,83616

Table 2. Simulation parameters

Number of cells (fluid)	247240
Number of elements (structure)	900
Type of structural element	*Hexa-8 with ESF*
Force magnitude (N)	$1,0 \cdot 10^5$
Flow velocity u (m/s)	0,0
Flow velocity v (m/s)	0,0
Flow velocity w (m/s)	0,0

2.2 Hexa-8 with Extra Shape Functions element for FEM in structural subsystem

To solve a case using MEF, you must choose polynomial shape functions. The degrees of polynomials used are related to the number of nodal unknowns of each element. The standard Hexa-8 element interpolation functions (linear) are insufficient to describe the behavior of a bending beam.

In the search for higher degree interpolation functions that did not significantly increase the computational cost, incompatible (or non-conforming) elements were proposed by Taylor (1976). In the works of Alwathaf (2014) and Mandal and Dewangan (2017) incompatible elements are used to solve cases of beam subjected to static forces. These elements add a quadratic term to the shape functions for standard trilinear element Hexa-8. In Eq. 1 are shown the shape functions of an incompatible Hexa-8 element.

$$\begin{aligned} x &= \sum_{i=1}^{8} N_i(\xi,\eta,\zeta)x_i + [P]\{\alpha\}, \\ y &= \sum_{i=1}^{8} N_i(\xi,\eta,\zeta)y_i + [P]\{\alpha\}, \\ z &= \sum_{i=1}^{8} N_i(\xi,\eta,\zeta)z_i + [P]\{\alpha\}, \end{aligned} \tag{1}$$

where $[P]$ are the additional incompatible modes, which will be used to correct the displacement error, and this term is defined in a matrix form as follows:

$$[P] = \begin{bmatrix} P1 & P2 & P3 & 0 & 0 & 0 & 0 & 0 & 0 \\ 0 & 0 & 0 & P1 & P2 & P3 & 0 & 0 & 0 \\ 0 & 0 & 0 & 0 & 0 & 0 & P1 & P2 & P3 \end{bmatrix} \tag{2}$$

where:

$$P_1 = (1-\xi^2); \quad P_2 = (1-\eta^2); \quad P_3 = (1-\zeta^2), \tag{3}$$

and,

$$\alpha^T = \begin{bmatrix} \alpha_1 & \alpha_2 & \alpha_3 & \alpha_4 & \alpha_5 & \alpha_6 & \alpha_7 & \alpha_8 & \alpha_9 \end{bmatrix}, \tag{4}$$

where $\alpha_1 \ldots \alpha_9$ are constants that are a function of the element's dimension, curvature and Poisson's ratio.

To determine the deformation matrix $[B]$ (Eq. 5) composed of partial derivatives of the shape functions, which are a function of the local natural coordinate system (ξ, η, ζ), it must apply the chain law (Eq. 6) using the Jacobian matrix $[J]$ (Eq. 8).

$$B_i = LN_i = \begin{bmatrix} \frac{\partial N_i}{\partial x} & 0 & 0 \\ 0 & \frac{\partial N_i}{\partial y} & 0 \\ 0 & 0 & \frac{\partial N_i}{\partial z} \\ 0 & \frac{\partial N_i}{\partial z} & \frac{\partial N_i}{\partial y} \\ \frac{\partial N_i}{\partial z} & 0 & \frac{\partial N_i}{\partial x} \\ \frac{\partial N_i}{\partial y} & \frac{\partial N_i}{\partial x} & 0 \end{bmatrix} \tag{5}$$

$$\begin{aligned} \frac{\partial N_i}{\partial \xi} &= \frac{\partial N_i}{\partial x}\frac{\partial x}{\partial \xi} + \frac{\partial N_i}{\partial y}\frac{\partial y}{\partial \xi} + \frac{\partial N_i}{\partial z}\frac{\partial z}{\partial \xi}, \\ \frac{\partial N_i}{\partial \eta} &= \frac{\partial N_i}{\partial x}\frac{\partial x}{\partial \eta} + \frac{\partial N_i}{\partial y}\frac{\partial y}{\partial \eta} + \frac{\partial N_i}{\partial z}\frac{\partial z}{\partial \eta}, \\ \frac{\partial N_i}{\partial \zeta} &= \frac{\partial N_i}{\partial x}\frac{\partial x}{\partial \zeta} + \frac{\partial N_i}{\partial y}\frac{\partial y}{\partial \zeta} + \frac{\partial N_i}{\partial z}\frac{\partial z}{\partial \zeta}, \end{aligned} \tag{6}$$

Which can be expressed in matrix form as:

$$\begin{Bmatrix} \frac{\partial N_i}{\partial \xi} \\ \\ \frac{\partial N_i}{\partial \eta} \\ \\ \frac{\partial N_i}{\partial \zeta} \end{Bmatrix} = J \begin{Bmatrix} \frac{\partial N_i}{\partial x} \\ \\ \frac{\partial N_i}{\partial y} \\ \\ \frac{\partial N_i}{\partial z} \end{Bmatrix} \tag{7}$$

where the Jacobian matrix is defined as:

$$J = \begin{bmatrix} \frac{\partial x}{\partial \xi} & \frac{\partial y}{\partial \xi} & \frac{\partial z}{\partial \xi} \\ \frac{\partial x}{\partial \eta} & \frac{\partial y}{\partial \eta} & \frac{\partial z}{\partial \eta} \\ \frac{\partial x}{\partial \zeta} & \frac{\partial y}{\partial \zeta} & \frac{\partial z}{\partial \zeta} \end{bmatrix} \tag{8}$$

and its inverse is defined as:

$$J^{-1} = \begin{bmatrix} J_{11}^* & J_{12}^* & J_{13}^* \\ J_{21}^* & J_{22}^* & J_{23}^* \\ J_{31}^* & J_{32}^* & J_{33}^* \end{bmatrix} \tag{9}$$

The deformation relationship can be written as a function of the derivatives of the shape functions and the displacements as:

$$\{\varepsilon\} = [B]\{d\} \tag{10}$$

where,

$$\{d\}^T = [u_1, v_1, w_1, \ldots, u_8, v_8, w_8, \alpha_1, \alpha_2, \alpha_3, \alpha_4, \alpha_5, \alpha_6, \alpha_7, \alpha_8, \alpha_9], \tag{11}$$

and

$$[B] = \Big[[B_1], \ldots, [B_8], [P_1^{'}], [P_2^{'}], [P_3^{'}]\Big], \tag{12}$$

The Eq. 10 can be written as:

$$\{\varepsilon\} = \sum_{i=1}^{8} [B_i]\{d_i\} + [P^{'}]\{\alpha^{'}\}, \tag{13}$$

or

$$\{\varepsilon\} = [B_a]\{d_a\} + [P^{'}]\{\alpha^{'}\}, \tag{14}$$

where

$$[B_a] = \Big[[B_1], [B_2], \ldots, [B_8]\Big], \tag{15}$$

$$\{d_a\}^T = [u_1, v_1, w_1, \ldots, u_8, v_8, w_8], \tag{16}$$

$$[P^{'}]\{\alpha^{'}\} = \begin{bmatrix} \frac{\partial P_1}{\partial x} & 0 & 0 & \frac{\partial P_2}{\partial x} & 0 & 0 & \frac{\partial P_3}{\partial x} & 0 & 0 \\ 0 & \frac{\partial P_1}{\partial y} & 0 & 0 & \frac{\partial P_2}{\partial y} & 0 & 0 & \frac{\partial P_3}{\partial y} & 0 \\ 0 & 0 & \frac{\partial P_1}{\partial z} & 0 & 0 & \frac{\partial P_2}{\partial z} & 0 & 0 & \frac{\partial P_3}{\partial z} \\ \frac{\partial P_1}{\partial y} & \frac{\partial P_1}{\partial x} & 0 & \frac{\partial P_2}{\partial y} & \frac{\partial P_2}{\partial x} & 0 & \frac{\partial P_3}{\partial y} & \frac{\partial P_3}{\partial x} & 0 \\ 0 & \frac{\partial P_1}{\partial z} & \frac{\partial P_1}{\partial y} & 0 & \frac{\partial P_2}{\partial z} & \frac{\partial P_2}{\partial y} & 0 & \frac{\partial P_3}{\partial z} & \frac{\partial P_3}{\partial y} \\ \frac{\partial P_1}{\partial z} & 0 & \frac{\partial P_1}{\partial x} & \frac{\partial P_2}{\partial z} & 0 & \frac{\partial P_2}{\partial x} & \frac{\partial P_3}{\partial z} & 0 & \frac{\partial P_3}{\partial x} \end{bmatrix} \begin{Bmatrix} \alpha_1 \\ \alpha_4 \\ \alpha_7 \\ \alpha_2 \\ \alpha_5 \\ \alpha_8 \\ \alpha_3 \\ \alpha_6 \\ \alpha_9 \end{Bmatrix} \tag{17}$$

Derivatives of additional shape functions can be written as follows:

$$\frac{\partial P_i}{\partial x} = J_{11}^* \frac{\partial P_i}{\partial \xi} + J_{12}^* \frac{\partial P_i}{\partial \eta} + J_{13}^* \frac{\partial P_i}{\partial \zeta},$$

$$\frac{\partial P_i}{\partial y} = J_{21}^* \frac{\partial P_i}{\partial \xi} + J_{22}^* \frac{\partial P_i}{\partial \eta} + J_{23}^* \frac{\partial P_i}{\partial \zeta}, \tag{18}$$

$$\frac{\partial P_i}{\partial z} = J_{31}^* \frac{\partial P_i}{\partial \xi} + J_{32}^* \frac{\partial P_i}{\partial \eta} + J_{33}^* \frac{\partial P_i}{\partial \zeta},$$

Thus, the matrix $[P^{'}]$ is defined as follows:

$$[P^{'}] = \begin{bmatrix} -2\xi J_{11}^{*} & 0 & 0 & -2\eta J_{12}^{*} & 0 & 0 & -2\zeta J_{13}^{*} & 0 & 0 \\ 0 & -2\xi J_{21}^{*} & 0 & 0 & -2\eta J_{22}^{*} & 0 & 0 & -2\zeta J_{23}^{*} & 0 \\ 0 & 0 & -2\xi J_{31}^{*} & 0 & 0 & -2\eta J_{32}^{*} & 0 & 0 & -2\zeta J_{33}^{*} \\ -2\xi J_{21}^{*} & -2\xi J_{11}^{*} & 0 & -2\eta J_{22}^{*} & -2\eta J_{12}^{*} & 0 & -2\zeta J_{23}^{*} & -2\zeta J_{13}^{*} & 0 \\ 0 & -2\xi J_{31}^{*} & -2\xi J_{21}^{*} & 0 & -2\eta J_{32}^{*} & -2\eta J_{22}^{*} & 0 & -2\zeta J_{33}^{*} & -2\zeta J_{23}^{*} \\ -2\xi J_{31}^{*} & 0 & -2\xi J_{11}^{*} & -2\eta J_{32}^{*} & 0 & -2\eta J_{12}^{*} & -2\zeta J_{33}^{*} & 0 & -2\zeta J_{13}^{*} \end{bmatrix} \tag{19}$$

The calculation of the elementary stiffness matrix is performed using Eq. 20. With the addition of the incompatible modes the stiffness matrix calculation is now calculated with Eq. 21. The stiffness matrix is then subdivided into four submatrices (K_{aa},$K_{a\alpha}$,$K_{\alpha a}$ and $K_{\alpha\alpha}$). In Eq. 23 the elementary equilibrium equation is shown.

$$[K_e] = \iiint_{V_e} [B]^T [D][B] dV_e \tag{20}$$

$$[K_e] = \iiint_{V_e} \begin{bmatrix} [B_a]^T \\ [P^{'}]^T \end{bmatrix} \Big[D\Big] \begin{bmatrix} [B_a] & [P^{'}] \end{bmatrix} dV_e \tag{21}$$

$$[K_e] = \iiint_{V_e} \begin{bmatrix} \Big[[B_a]^T [D][B_a]\Big] & \Big[[B_a]^T [D][P^{'}]\Big] \\ \Big[[P^{'}]^T [D][B_a]\Big] & \Big[[P^{'}]^T [D][P^{'}]\Big] \end{bmatrix} dV_e \tag{22}$$

$$\begin{bmatrix} [K_{aa}]_{24x24} & [K_{a\alpha}]_{24x9} \\ [K_{\alpha a}]_{9x24} & [K_{\alpha\alpha}]_{9x9} \end{bmatrix} \begin{Bmatrix} \{d_a\}_{24x1} \\ \{\alpha\}_{9x1} \end{Bmatrix} = \begin{Bmatrix} \{F_a\}_{24x1} \\ \{0\}_{9x1} \end{Bmatrix} \tag{23}$$

To remove non-nodal displacements (α) static condensation is used, which is derived in Eq. 24.

$$\Big[[K_{\alpha\alpha}] - [K_{a\alpha}][K_{\alpha\alpha}]^{-1}[K_{\alpha a}]\Big] d_a = F_a \tag{24}$$

Therefore, the condensed elementary stiffness matrix to be used by the incompatible element theory is shown in Eq. 25.

$$[K_e] = \iiint_{V_e} \left[\Big[[B_a]^T [D][B_a]\Big] - \Big[[B_a]^T [D][P^{'}]\Big] \Big[[P^{'}]^T [D][P^{'}]\Big]^{-1} \Big[[P^{'}]^T [D][B_a]\Big] \right] dV_e \tag{25}$$

The elementary mass matrix is calculated with Eq. 26.

$$[M_e] = \iiint_{V_e} \rho [N]^T [N] \, dV_e \tag{26}$$

Transforming the Eq. 25 and 26 to the isoparametric coordinate system (ξ,η,ζ) obtains the Eq. **??** and 28.

$$[K_e] = \int_{-1}^{+1} \int_{-1}^{+1} \int_{-1}^{+1} \left[\Big[[B_a]^T [D][B_a]\Big] - \Big[[B_a]^T [D][P^{'}]\Big] \Big[[P^{'}]^T [D][P^{'}]\Big]^{-1} \Big[[P^{'}]^T [D][B_a]\Big] \right] det[\mathbf{J}] \, d\xi \, d\eta \, d\zeta \tag{27}$$

$$[M_e] = \int_{-1}^{+1} \int_{-1}^{+1} \int_{-1}^{+1} \rho [N]^T [N] det[\mathbf{J}] \, d\xi \, d\eta \, d\zeta \tag{28}$$

The solutions for Eq. 27 and 28 can be obtained through the use of numerical Gauss integration, which for an element of 8 nodes, two integration points would be sufficient. The three-dimensional Gauss numerical integration is shown in Eq. 29.

$$I = \int_{-1}^{+1} \int_{-1}^{+1} \int_{-1}^{+1} f(\xi, \eta, \zeta) d\xi d\eta d\zeta = \sum_{i=1}^{n} \sum_{j=1}^{m} \sum_{k=1}^{l} = w_i w_j w_k f(\xi_i, \eta_j, \zeta_k), \tag{29}$$

where, w_i, w_j and w_k are the weight functions that depend on the number of quadrature points and f is the function in the isoparametric natural coordinates.

2.3 Fluid Subsystem

Simplifications must be made to guarantee the solution of the problem, for this case, the flow was considered incompressible and stationary, that is, without speed, which guarantees that the plate will be submerged in the fluid.

For the fluid subsystem, several computational methods were used for its solution. For the pressure-velocity coupling, the method of fractional steps was used, the advective model used was the CUBISTA proposed by Chorin (1968) and the temporal discretization method chosen was the semi-implicit method MCNAB (modified Crack-Nicolson / Adams-Bashford).

2.4 FSI coupling

The fluid-structure coupling, in partitioned way, is possible by solving the fluid and structural subsystems using FVM and FEM methods, and coupled through the immersed boundary method. This coupling can be strong or weak. The immersed frontier method allows the determination of those produced by the flow under the structure, which would be the source term of the momentum conservation equation (Navier-Stokes).

For the implementation of the immersed boundary method, a complementary STL (Standard Triangle Language) mesh is needed, the size of the elements of this mesh is calculated as a function of the size of the cells of the highest level of refinement. To carry out the transmission of forces, each element of the FEM mesh searches around it and finds the points of the STL mesh with which they are in contact, after identifying the points of the lagrangian mesh, the forces related to such points are interpolated and distributed in the respective nodes of the FEM mesh.

The algorithm used in the weak coupling of FSI is presented below in Algorithm 1.

Algorithm 1 Weak FSI coupling

while do$(t < t_{max}$ and $n < n_{max})$

$t^{n+1} = t^n + \Delta t$

$(\dots)$ Solve fluid subsystem

$F_{flow}^{n+1} = F_{flow}\left(v^*(\vec{x}), \begin{Bmatrix} u(\vec{x}_k) \\ \dot{u}(\vec{x}_k) \end{Bmatrix}^n\right)$

$\begin{bmatrix} u(\vec{x}_k) \\ \dot{u}(\vec{x}_k) \end{bmatrix}^{n+1}$= PV $\left(\mathrm{t}^n, \Delta t, F_{flow}^{n+1}\right)$ Pressure-velocity coupling

$(\dots)$ Solve structure subsystem

$n = n + 1$

3. Results

In Fig. 1 the computational mesh used in the simulations is shown. A mesh of five levels of refinement from a base mesh of 32 x 16 x 16 was used for the fluid subsystem as shown in Fig. 2.

For comparison purposes with the experimental data obtained by Lindholm *et al.* (1965), in this work the dimensionless frequency parameter is used. Dimensionless frequencies are calculated with Eq. 30.

The cases were simulated during $5\ s$. In the tests, the damped natural frequencies were calculated for the plates described above in vacuum and submerged in air and water. Theoretical results obtained by Lindholm *et al.* (1965) and the results obtained through computational simulation using the *Hexa-8 with ESF* element were comparated.

$$\Omega = \frac{\omega_n}{(D/\rho_p h a^4)^{1/2}}, \tag{30}$$

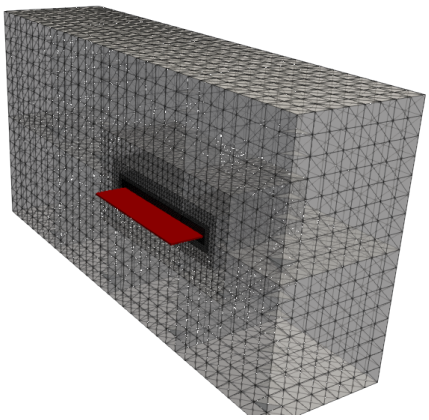

Figure 1. Meshes used for Lind-6 plate

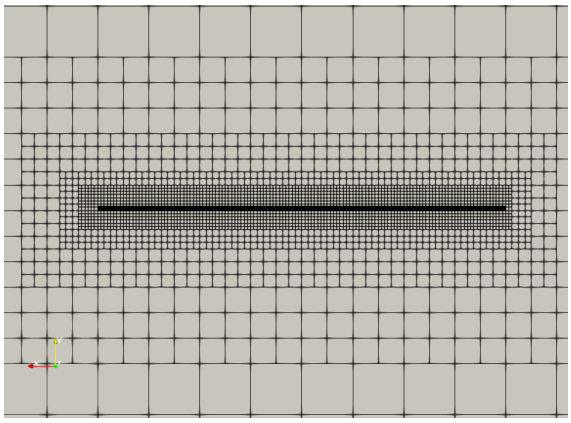

Figure 2. Refinement levels of fluid computational mesh used in Lind-6

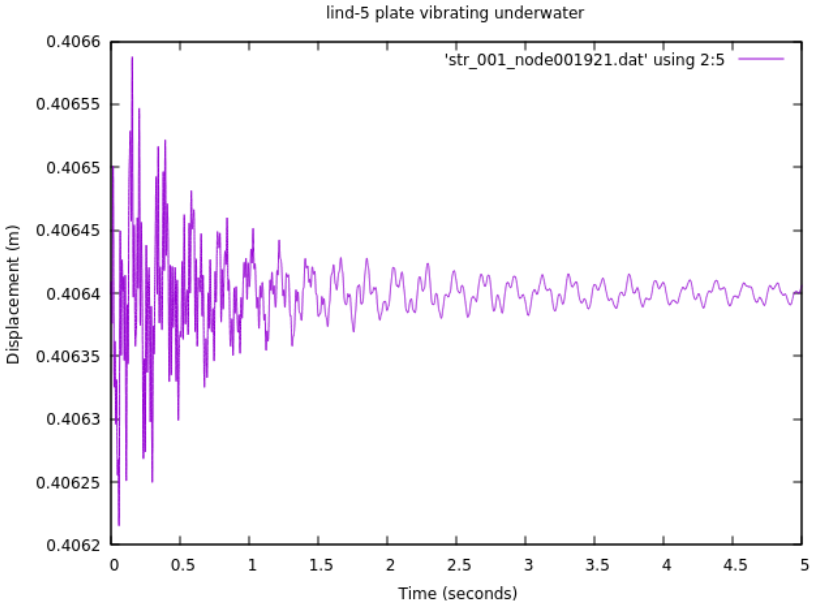

Figure 3. Displacement in time in y direction for Lind-5 plate.

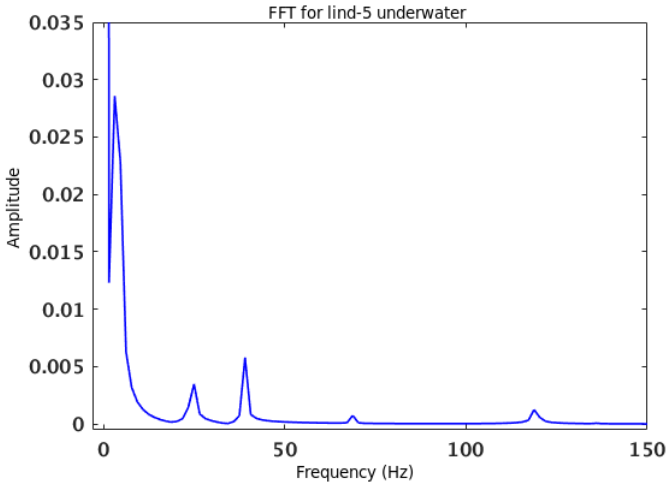

Figure 4. FFT for Lind-5 plate submerged in air.

For visualization purposes, in Figs. 5 and 6, the images of the resulting lines and the pressure field at the free end of the plate, resulting from the vibration of the structure after the application of the instantaneous force, are arranged.

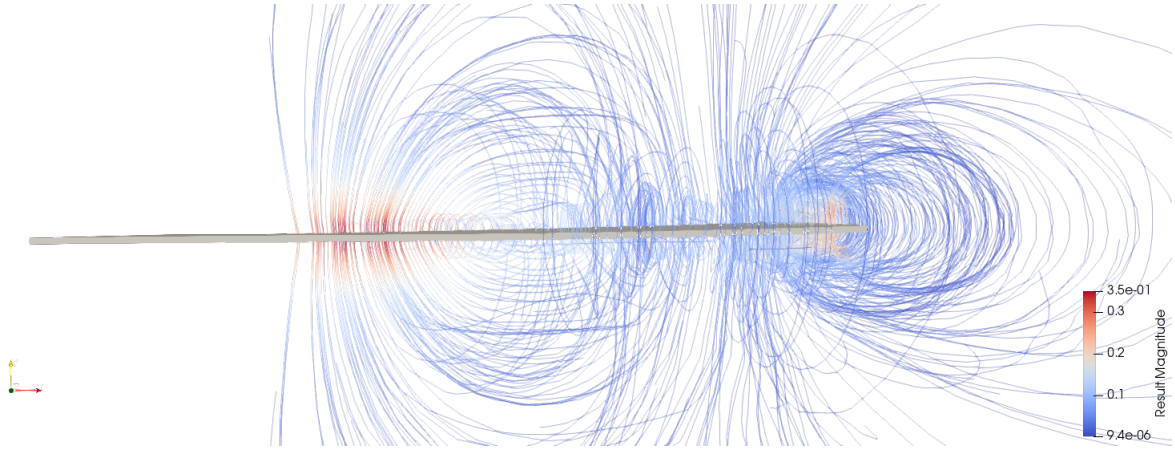

Figure 5. Velocity streamlines for Lind-7 plate. Side view.

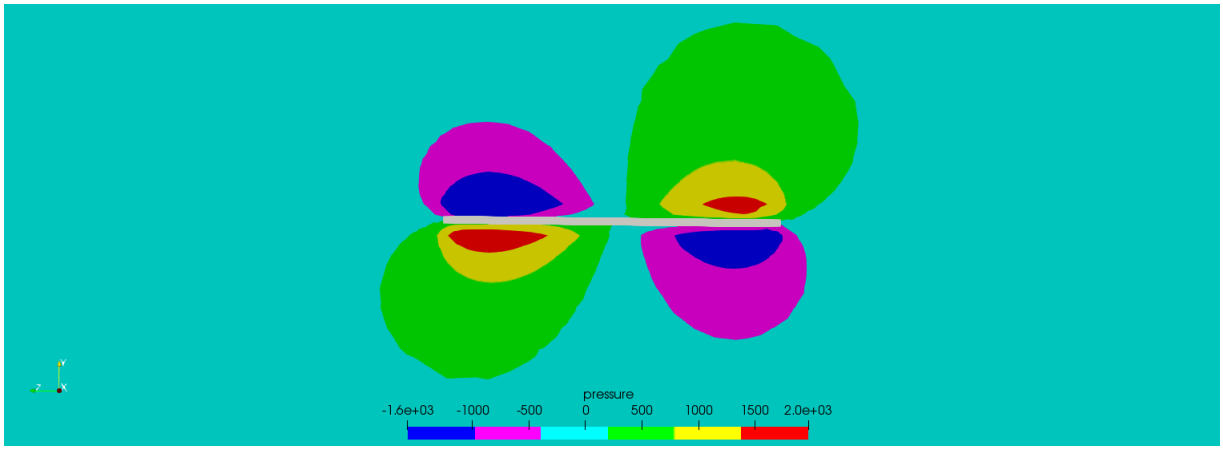

Figure 6. Pressure field at the free end for Lind-7 plate. Frontal view.

Next, in Tabs. 3 to 6, the errors related to the experimental results obtained by Lindholm *et al.* (1965) for the dimensionless frequencies obtained through of the simulations in each case.

Table 3. Dimensionless frequency errors in relation to the Lind-5 plate material experiment

Lind-5	Lindholm *et al.* (1965)	Present work	Relative error
Vacuum	3,321	3,360	1,17 %
	8,313	8,436	1,48 %
	20,386	21,121	3,61 %
	26,974	27,575	2,23 %
	29,872	31,287	4,74 %
Air	3,322	3,449	3,84 %
	8,313	8,379	0,79 %
	20,386	20,455	0,34 %
	26,974	27,109	0,50 %
	29,872	30,044	0,58 %
Water	1,773	1,798	1,40 %
	5,312	5,033	5,26 %
	12,245	12,225	0,17 %
	18,420	16,899	8,26 %
	20,179	19,058	5,56 %

Table 4. Dimensionless frequency errors in relation to the Lind-6 plate material experiment

Lind-6	Lindholm *et al.* (1965)	Present work	Relative error
Vacuum	3,406	3,409	0,02 %
	14,625	14,695	0,47 %
	21,248	21,266	0,08 %
	47,878	47,856	0,05 %
	57,950	59,796	3,18 %
Air	3,339	3,558	6,57 %
	14,901	14,750	1,02 %
	20,834	21,869	4,97 %
	48,016	48,305	0,60 %
	58,226	61,013	4,79 %
Water	1,670	1,427	14,55 %
	9,313	8,563	8,06 %
	11,038	11,418	3,44 %
	30,631	28,547	6,80 %
	33,528	32,824	2,10 %

Table 5. Dimensionless frequency errors in relation to the Lind-7 plate material experiment

Lind-7	Lindholm *et al.* (1965)	Present work	Relative error
Vacuum	3,384	3,410	0,79 %
	21,141	21,002	0,66 %
	21,172	21,324	0,71 %
	66,435	65,998	0,66 %
	57,743	59,988	3,89 %
Air	3,353	3,111	7,22 %
	21,019	20,744	1,30 %
	20,769	20,744	0,12 %
	65,504	66,373	0,96 %
	58,364	58,923	1,33 %
Water	1,583	1,416	10,57 %
	12,915	11,325	12,31 %
	10,338	9,909	4,14 %
	40,668	35,391	12,98 %
	30,703	29,731	3,16 %

Table 6. Dimensionless frequency errors in relation to the Lind-8 plate material experiment

Lind-8	Lindholm *et al.* (1965)	Present work	Relative error
Vacuum	3,389	3,390	0,04 %
	34,063	33,763	0,88 %
	21,128	21,275	0,70 %
	104,344	103,462	0,85 %
	57,777	59,995	3,84 %
Air	3,311	3,018	8,85 %
	33,718	33,692	0,08 %
	20,869	21,567	3,35 %
	104,344	102,447	1,82 %
	58,726	59,304	0,98 %
Water	1,535	1,483	3,37 %
	20,869	20,610	1,24 %
	9,917	9,458	4,35 %
	64,849	64,504	0,53 %
	28,889	26,302	8,96 %

The results presented above shows that despite the great slenderness on plates, the three-dimensional element Hexa-8 ESF can represent the proposed physical case with a good quality, relatively high errors presented in plates submerged in water can possibly be related to high slenderness of the elements due the quantity of elements was constant of 900 elements for all the plates tested, better results can be obtained with a finer mesh, taking into account that there is a mesh refinement limit so as not to fall into error due to shear locking (when the element size is in the order of micrometers). These results were part of a validation process for this type of element for implementation into MFSim software. Using FEM with Hexa-8 with ESF element theory, for the FSI cases presented above, was demonstrated to be efficient enough in this paper. The implementations were carried out in FORTRAN 90 programming language, where more than 4000 lines of code were written and introduced in MFSim, of which 2 modules and 30 subroutines are part.

4. ACKNOWLEDGEMENTS

I would like to thank the Fluid Mechanics Laboratory (MFLab), the Federal University of Uberlandia (UFU) and the CAPES research funding organization.

5. REFERENCES

Alwathaf, A.H., 2014. "Development of 3D Finite Element Code of Incompatible Displacement Mode for Flexural Analysis". *Arabian Journal for Science and Engineering*, Vol. 39, No. 8, pp. 6009–6016.

Chorin, A.J., 1968. "Numerical Solution of the Navier-Stokes". *Mathematics of computation*, Vol. 22, No. 104, pp. 745–762.

Lindholm, U., Kana, D., Chu, W. and Abramson, H., 1965. "Elastic Vibration Characteristics of Cantilever Plates in Water". *Journal of Ship Research*, Vol. 9, No. 1, p. 123. URL `http://oai.dtic.mil/oai/oai?verb=getRecordmetadataPrefix=htmlidentifier=AD0643240`.

Mandal, R.R. and Dewangan, U.K., 2017. "Finite element modeling of beam with eight noded brick element using MATLAB". *International Journal of Civil Engineering and Technology*, Vol. 8, No. 5, pp. 646–656.

Sotiropoulos, F. and Yang, X., 2014. "Immersed boundary methods for simulating fluid-structure interaction". *Progress in Aerospace Sciences*, Vol. 65, pp. 1–21. ISSN 03760421. doi:10.1016/j.paerosci.2013.09.003. URL `http://dx.doi.org/10.1016/j.paerosci.2013.09.003`.

Taylor, R.L., 1976. "A non-conforming element for stress analysis". *International Journal for Numerical Methods in Engineering*, Vol. 10, pp. 1211–1219.

6. RESPONSIBILITY NOTICE

The following text, properly adapted to the number of authors, must be included in the last section of the paper:
The author(s) is (are) solely responsible for the printed material included in this paper.